

# Biorenewable Calcite as an Inorganic Filler in Ionic Liquid Gel Polymer Electrolytes for Supercapacitors

Jennifer N. Murphy,\* Tiago Mendes, Francesca M. Kerton, and Douglas R. MacFarlane

Cite This: *ACS Omega* 2023, 8, 21418–21424

Read Online

ACCESS |



Metrics &amp; More

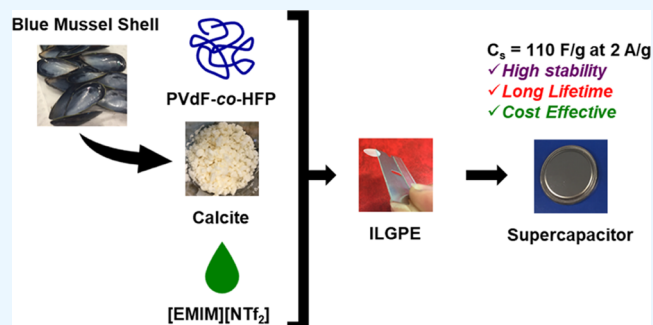


Article Recommendations



Supporting Information

**ABSTRACT:** Supercapacitors play a crucial role in the global shift toward cleaner, renewable energy and away from fossil fuels. Ionic liquid electrolytes have a larger electrochemical window than some organic electrolytes and have been mixed with various polymers to make ionic liquid gel polymer electrolytes (ILGPEs), a solid-state electrolyte and separator combination. One way to improve the conductivity of these electrolytes is to add inorganic materials such as ceramics and zeolites to increase their ionic conductivity. Herein, we incorporate a biorenewable calcite from waste blue mussel shells as an inorganic filler in ILGPEs. ILGPEs composed of 80 wt % [EMIM][NTf<sub>2</sub>] and 20 wt % PVdF-co-HFP are prepared with various amounts of calcite to determine the effect on the ionic conductivity. The optimal addition of calcite is 2 wt % based on the mechanical stability of the ILGPE. The ILGPE with calcite has the same thermostability (350 °C) and electrochemical window (3.5 V) as the control ILGPE. Symmetric coin cell capacitors were fabricated using ILGPEs with 2 wt % calcite and without calcite as a control. Their performance was compared using cyclic voltammetry and galvanostatic cycling. The specific capacitances of the two devices are similar, 110 and 129 F g<sup>-1</sup>, with and without calcite, respectively.



## INTRODUCTION

With the global abuse of fossil fuels to power modern civilization leading to limited resources and climate change, a global shift toward sustainable and renewable resources is more urgent than ever.<sup>1</sup> Energy systems play a large role in our lives, so electrical storage systems, such as batteries and electrochemical capacitors (ECs), are at the forefront of renewable energy.<sup>2</sup> ECs or supercapacitors are high-power-density charge-storage devices with a longer cycle life than that of rechargeable batteries, which stems from the electrostatic process at the electrode–electrolyte interface.<sup>3</sup> They are used in applications ranging from portable electronics to electric vehicles and even heavy machinery. ECs are safer during rapid charging and discharging compared to batteries. While often used in a circuit accompanying a battery, ECs can replace batteries in applications where high delivery or uptake, or power is required.<sup>2</sup> However, the energy storage capacity is lower than that of batteries.

In order to improve the performance of ECs, there are two components of the device one can alter: the electrode material and the electrolyte. Energy density is directly proportional to the square of the potential,  $E = 1/2 CV^2$ , where  $C$  is the capacitance and  $V$  is the potential. Aqueous electrolytes are limited to a potential of approximately 1 V.<sup>4</sup> While the maximum potential of 2.7 V for organic electrolytes is much higher, their flammability and toxicity make organic electrolytes hazardous.<sup>5</sup> Therefore, investigating electrolytes with

higher operating potentials while also being inherently safer is attractive for clean energy applications. Ionic liquids (ILs) have high conductivities and wider electrochemical windows than organic and aqueous electrolytes and have been explored as electrolytes in supercapacitors to increase the maximum cell voltage, thereby increasing the maximum energy density.<sup>5–8</sup> ILs are chemically and thermally stable and their non-flammability and negligible volatility make them inherently safer than organic electrolytes.

Even though ILs are much more viscous than organic and aqueous electrolytes, a leakage risk still exists for ECs. The construction of a safe and secure electrochemical device hinges on removing this risk of leakage. ILs have been used to make gel polymer electrolytes, a combination of polymer and IL, where the IL is entrapped in the polymer, making a solid-state electrolyte/separator with additional mechanical and interfacial stability than typical electrolytes.<sup>9,10</sup> Solid electrolytes reduce the leaking of ECs and help to maintain good electrode–electrolyte contact.<sup>11</sup> Ionic liquid-based gel polymer electro-

Received: October 25, 2022

Accepted: March 2, 2023

Published: June 7, 2023



lytes (ILGPEs) have been synthesized using a plethora of ionic liquids and polymer combinations and used in lithium batteries and electrochemical supercapacitors.<sup>12–14</sup> Research has shown that the chemical and mechanical stability and conductivity of ILGPEs can be improved further with the addition of passive inorganic fillers (one that is not involved in the conduction process) such as ceramics (i.e., SiO<sub>2</sub>) and zeolites.<sup>10,12,15,16</sup> These fillers can also act as a diluent and reduce the cost of the ILGPE.

Many reports have focused on the renewability of the carbon electrode material through the conversion of biomass to porous carbon for electrodes for ECs.<sup>7,17</sup> To the best of our knowledge, we are the first to consider the sustainability of an inorganic or ceramic filler component that can be used in order to improve the stability or mechanical properties of the ILGPE and reduce the cost. Recently, in the work of one of the authors, a biorenewable calcite material was isolated from waste blue mussel shells.<sup>18</sup> Unlike the hard and brittle calcite that makes up mussel shells, this expanded calcite is soft and compressible with a texture similar to that of candy floss. Herein, we describe the addition of this sustainable inorganic filler into ILGPEs made with 1-ethyl-3-methylimidazolium bis(trifluoromethylsulfonyl)imide [EMIM][NTf<sub>2</sub>] and poly(vinylidene fluoride)-*co*-hexafluoropropylene (PVdF-*co*-HFP). The effects of the addition of the calcite on the ILGPE were investigated using electrochemical impedance spectroscopy (EIS), infrared spectroscopy (IR), thermogravimetric analysis (TGA), differential scanning calorimetry (DSC), and scanning electron microscopy (SEM). Symmetric coin cell capacitors were fabricated using the ILGPE with and without calcite for direct comparison purposes. The performance of the ECs was studied by EIS, cyclic voltammetry (CV), and galvanostatic charge–discharge cycling.

## EXPERIMENTAL SECTION

**Materials.** 1-Ethyl-3-methylimidazolium bis(trifluoromethylsulfonyl)imide [EMIM][NTf<sub>2</sub>] (99.9%) was purchased from Solvionic. Acetone was purchased from Univar (>99.5%). Poly(vinylidene fluoride)-*co*-hexafluoropropylene (PVdF-*co*-HFP), poly(vinylidene fluoride) (PVdF) powder, and *N*-methyl-2-pyrrolidone (NMP) were purchased from Sigma Aldrich. Vulcan XC-72R (carbon black) was purchased from the Fuel cell store. TF-B520, the activated carbon for the electrodes, was purchased from the MTI Corporation. All chemicals were used without further purification.

**Ionic Liquid Gel Polymer Electrolytes.** Initial screening showed that the minimum amount of PVdF-*co*-HFP needed to make stable, fully solid films was 20 wt %. Therefore, the films reported herein all have an [EMIM][NTf<sub>2</sub>]/PVdF-*co*-HFP ratio of 4:1. PVdF-*co*-HFP was dissolved in acetone at 50 °C with stirring before adding [EMIM][NTf<sub>2</sub>]. The clear colorless solution was stirred and heated until approximately half of the solvent evaporated. At this point, if the film was to include calcite, calcite would be added and stirred vigorously with continued heating. The wt % of calcite added was relative to the combined mass of [EMIM][NTf<sub>2</sub>] and PVdF-*co*-HFP. The films were cast onto a large glass plate 1000 μm doctor blade when there was very little solvent left and dried in a vacuum oven overnight at 60 °C. The resulting films were between 100 and 160 μm thick and cut into spheres with a 9.72 mm diameter for supercapacitor fabrication.

**Electrode Preparation.** Electrodes were prepared using 80% TF-B520 (activated carbon), 10% Vulcan XC-72R

(carbon black), and 10% PVdF powder (binder) by weight. The PVdF was dissolved in a minimal amount of NMP. The carbon materials were ground in an agate mortar and pestle very vigorously before being added to the clear colorless PVdF solution. The black mixture remained viscous and was stirred at room temperature for 20 h before being cast onto an aluminum foil current collector using a 100 μm doctor blade. The film was dried in a vacuum oven at 110 °C for 24 h before being cut into 6.35 mm disks. The disks were dried further in a vacuum oven before being transferred to an argon glovebox for supercapacitor fabrication. The mass of active carbon materials on each electrode was 1 mg/cm<sup>2</sup>.

**Electrochemical Measurements.** The ionic conductivity of the ILGPEs was measured by AC impedance spectroscopy using an MTZ-35 BioLogic instrument. The films were loaded into a barrel cell equipped with two stainless steel electrodes with a surface area of 4.15 cm<sup>2</sup>. The temperature of the barrel cell was controlled with a Eurotherm 2204e temperature controller. The conductivity was measured from 25 to 80 °C in 10 °C increments from 30 °C with a hold of 5 min before the measurement commenced at frequencies ranging from 1.0 Hz to 10 MHz using a signal voltage of 0.1 V.

To make the supercapacitors, the ILGPEs were employed as the electrolyte separator and as such were sandwiched between two symmetric electrodes with a diameter of 6.35 mm. The electrodes were made with commercially available carbon materials using the slurry coating method onto an aluminum foil. The coin cell supercapacitors were fabricated in an argon glovebox. Galvanostatic charge–discharge tests were performed using a NEWARE battery testing system from 0 to 3 V at current densities ranging from 0.5 to 7 A g<sup>-1</sup>. Five thousand cycles of the devices at 2.5 V with a current density of 2 A g<sup>-1</sup> were completed to assess the stability and lifetime of the supercapacitors. Specific capacitances from galvanostatic testing were calculated using  $C = 2(I\Delta t/m\Delta V)$ , where  $I$  is the constant discharge current,  $\Delta t$  is the discharging time,  $m$  is the mass of one electrode, and  $\Delta V$  is the voltage window upon discharging. The energy density ( $E$ ) and power density ( $P$ ) were then calculated using  $E = [C(\Delta V)^2]/8$  and  $P = E/\Delta t$ , where  $E$ ,  $C$ ,  $\Delta V$ ,  $P$ , and  $\Delta t$  are the specific energy, specific capacitance, potential window, specific power, and discharge time, respectively. A multichannel potentiostat from Princeton Applied Research VMP2 was used to perform electrochemical measurements on the fabricated supercapacitors. Cyclic voltammetry (CV) and electrochemical impedance spectroscopy (EIS) was performed using a two-electrode setup at room temperature. The CV experiments were conducted at scan rates of 25, 50, 100, and 200 mV s<sup>-1</sup> and voltages ranging from 0 to 4.0 V. The EIS was measured in a frequency range of 1 MHz to 0.01 Hz. Specific capacitance was calculated from the CVs according to  $C = i/s$ , where  $i$  is the average current and  $s$  is the scan rate.

**Characterization.** Thermogravimetric analysis (TGA) was performed with a Mettler Toledo TGA/DSC 1STARe at a heating rate of 10 °C min<sup>-1</sup> from 25–550 °C under a flow of N<sub>2</sub> (50 mL min<sup>-1</sup>). A DSC Q100 was used for differential scanning calorimetry (DSC) experiments, where the films were first cooled to –150 °C (with a 2 min isothermal hold) and then heated to 100 °C (with a 2 min isothermal hold). The heating and cooling rates were both 10 °C min<sup>-1</sup>. Three cycles were performed and the first was discarded. Fourier transform infrared spectra were obtained using a Bruker Equinox IFS 55 infrared spectrophotometer in attenuated total reflectance over

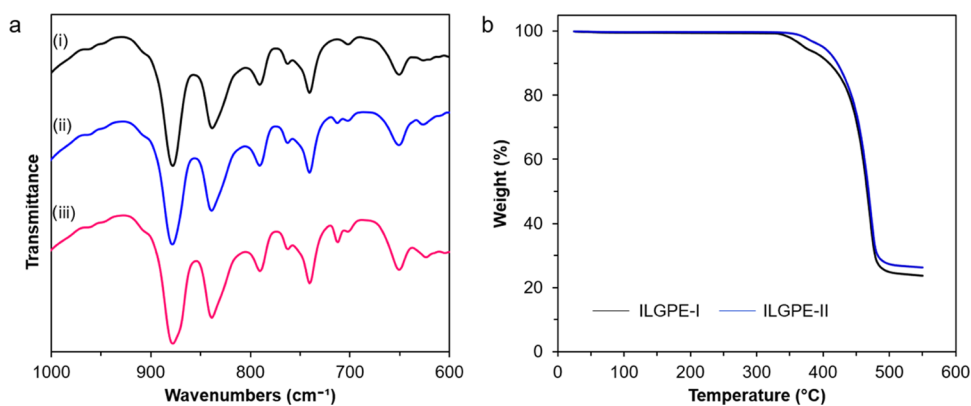


**Figure 1.** (a) FTIR spectra of ILGPEs to show the incorporation of calcite. (i) ILGPE-I, (ii) ILGPE-II, and (iii) ILGPE-III. (b) Thermogravimetric analysis of ILGPE-I and ILGPE-II.

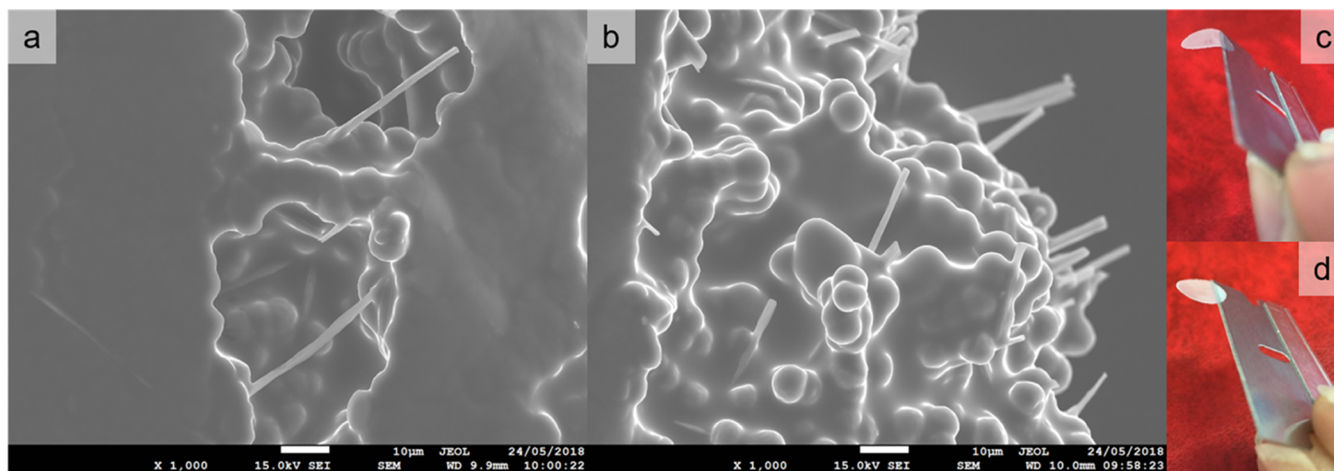


**Figure 2.** SEM micrographs of (a) porous region and (b) edge region of ILGPE-II and digital images of (c) ILGPE-III and (d) ILGPE-II.

64 scans with a resolution of  $4 \text{ cm}^{-1}$ . Dynamic mechanical analysis was performed using a Perkin Elmer DMA 800. The films were cooled to  $-130 \text{ }^\circ\text{C}$  rapidly and heated to  $30 \text{ }^\circ\text{C}$  at a rate of  $5 \text{ }^\circ\text{C min}^{-1}$ . Scanning electron microscopy (SEM) images from Memorial University were obtained using FEI MLA 650 FEG under a high vacuum ( $10^{-6}$  torr). The voltage ranged from 5 to 10 kV and the current was 10 mA at working distances ranging from 8.4–10.5 mm.

## RESULTS AND DISCUSSION

Investigation into the optimal amount of PVdF-co-HFP added to [EMIM][NTf<sub>2</sub>] for strong and flexible ILGPEs showed that at least 20 wt % of PVdF-co-HFP was required. Therefore, we studied the effect of adding varying amounts (0.5–4 wt %) of calcite from mussel shells as a percentage of the total mass of [EMIM][NTf<sub>2</sub>]/PVdF-co-HFP with the IL-to-polymer ratio of 80:20. An ILGPE control, [EMIM][NTf<sub>2</sub>]/PVdF-co-HFP with the IL-to-polymer ratio of 80:20 ratio but no calcite, was used for comparison purposes and is herein abbreviated as ILGPE-I.

**Ionic Conductivity.** The ILGPE films were 1–1.3 mm thick, and this made ionic conductivity measurements difficult to obtain. The addition of 0.5 and 1 wt % calcite had a negative effect on the conductivity and did not enhance the mechanical stability of the film (Figure S1). The best ILGPE film, with respect to being strong, flexible, and easy to handle and with minimal decline in ionic conductivity was the ILGPE with an IL-to-polymer ratio of 80:20 and 2 wt % calcite, abbreviated

here as ILGPE-II. Films with 4 wt % calcite PVdF-co-HFP (ILGPE-III) initially had good conductivity; however, this film was difficult to handle (not rigid) and would tear very easily. Therefore, we decided to move forward with ILGPE-I and -II for more in-depth characterization and fabrication of supercapacitors.

The ionic conductivity of ILGPE-I and -II at  $25 \text{ }^\circ\text{C}$  was  $4.3$  and  $2.7 \text{ mS cm}^{-1}$ , respectively. The ionic conductivities for these two films were measured in triplicate. An Arrhenius plot of the ionic conductivities can be found in Supporting Information, Figure S2. There is a decrease in the conductivity of ILGPE-II as expected because it has less IL than ILGPE-I. However, the ionic conductivity of ILGPE-II is still higher or on par with those of other ILGPEs containing imidazolium-based ILs, with or without inorganic additives,<sup>6,10,14,15,19</sup> especially considering that no ionic conductivity boosting compounds were added, such as metal salts, organic carbonates, and/or sulfolane.<sup>16,20</sup> Additionally, the ionic conductivity of  $2.7 \text{ mS cm}^{-1}$  for ILGPE-II is consistent with reports of polymer blend composite electrolytes used for Li-ion batteries that contain powdered  $\text{CaCO}_3$ .<sup>21</sup>

**Film Characterization Discussion.** Figure 1a shows the FTIR of three films, ILGPE-I, -II, and -III. All characteristic absorptions for calcite were convoluted by the [EMIM][NTf<sub>2</sub>] and PVdF-co-HFP except for one band at  $710 \text{ cm}^{-1}$ , which corresponds to the O–C–O bend of the  $\text{CO}_3^{2-}$  in calcite.<sup>22</sup> The intensity of this band increases as we add more calcite and

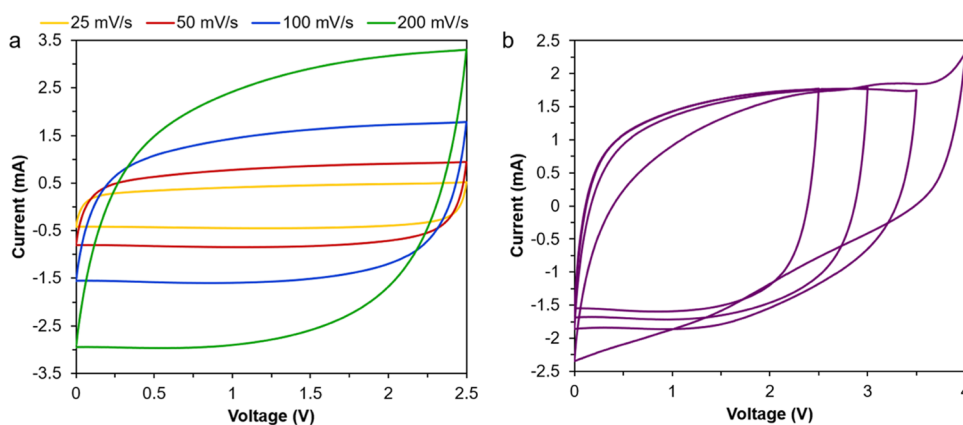


**Figure 3.** Cyclic voltammograms of Cell-II at (a) different scan rates and (b) different operating potentials at a scan rate of  $100 \text{ mV s}^{-1}$ .

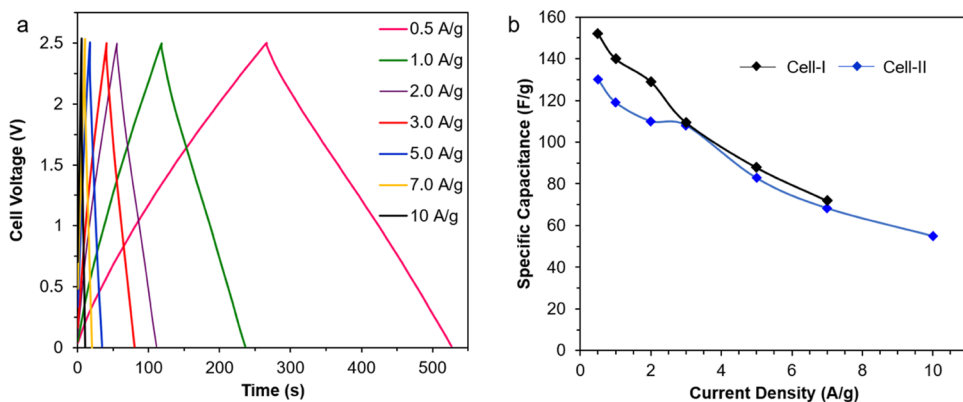


**Figure 4.** (a) Galvanostatic discharge curves for Cell-II at various current densities and (b) specific capacitance of Cell-I (black) and Cell-II (blue) as a function of current densities.

is absent in the control film, ILGPE-I. Thermogravimetric analysis of ILGPE-I and -II (Figure 1b) shows that the two films have near identical thermal stability and begin to decompose at  $350 \text{ }^\circ\text{C}$ . ILGPE-I and -II also have the same glass transition temperature of  $-95.0 \text{ }^\circ\text{C}$ , as determined by DSC (see Supporting Information, Figure S3), which suggests that the thermal properties of the two films are the same.

Surface morphologies of the ILGPEs were characterized by SEM. Figure 2 shows representative images of the surface and edges of ILGPE-II. There are very clear porous regions where the prismatic calcite is visible. The differences in the rigidity of ILGPE-III and ILGPE-II are shown in Figure 2c,d. ILGPE-III bends under its own weight, whereas ILGPE-II remains straight. Cross-sectional micrographs of ILGPE-I and -II are presented in Figure S4 (Supporting Information). The cross-sectional morphology is the same for both films. The calcite incorporation is homogeneous, and it is pointed along the plane of the film. That is, the calcite is pointed parallel to the surface and not pointed out of the film. The addition of calcite to the ILGPE changes the volume of the mixture. This changes the amount of IL per film and decreases the cost of the electrolyte by 17%. Electrochemical measurements were performed to assess the performance of ILGPE-II in comparison to ILGPE-I to see how the addition of calcite affects capacitance and cycling stability.

ILGPE-I and -II were used in the fabrication of symmetric electrochemical capacitors called Cell-I and -II, respectively, and subjected to the same electrochemical testing.

**Electrochemical Measurements.** Cyclic voltammetry was used to explore different operating potentials at a scan rate of  $100 \text{ mV s}^{-1}$  to determine the potential window of Cell-I and -II. Thirty cycles at each voltage were first performed to stabilize the supercapacitors. The results were very similar for supercapacitors, with the results for Cell-II shown in Figure 3a,b and those for Cell-I in Supporting Information, Figure S5. Above  $3.5 \text{ V}$ , the voltammogram is no longer rectangular and exhibits a sharp increase in current. This is likely due to the partial decomposition of the IL at this high voltage and the current becomes partly Faradic. Even though the electrochemical window of the pure IL has been reported to be  $4 \text{ V}$ ,<sup>10</sup> many have reported a limitation to the electrochemical window when the ILs are incorporated in GPEs.<sup>19</sup>

Figure 3a shows that while an increase in current is observed from  $25$  to  $200 \text{ mV s}^{-1}$ , the rectangular shape becomes increasingly distorted as a result of the more pronounced ohmic drop. The specific capacitance of Cell-I and -II as calculated from the CVs was very similar (Cell-I =  $153$ ,  $146$ ,  $133$ , and  $109 \text{ F g}^{-1}$  and Cell-II =  $147$ ,  $140$ ,  $129$ , and  $114 \text{ F g}^{-1}$  at  $25$ ,  $50$ ,  $100$ , and  $200 \text{ mV s}^{-1}$ , respectively).

Galvanostatic charge–discharge curves of both supercapacitors at current densities ranging from  $0.5$  to  $7 \text{ A g}^{-1}$  have a symmetric triangular shape that is distinctive of double-layer capacitors with a high Coulombic efficiency. Figure 4a shows that the charge–discharge curve of Cell-II is very symmetric with nearly linear charge and discharge behavior.

Specific capacitances as a function of current density for Cell-I and -II are shown in Figure 4b. The highest specific

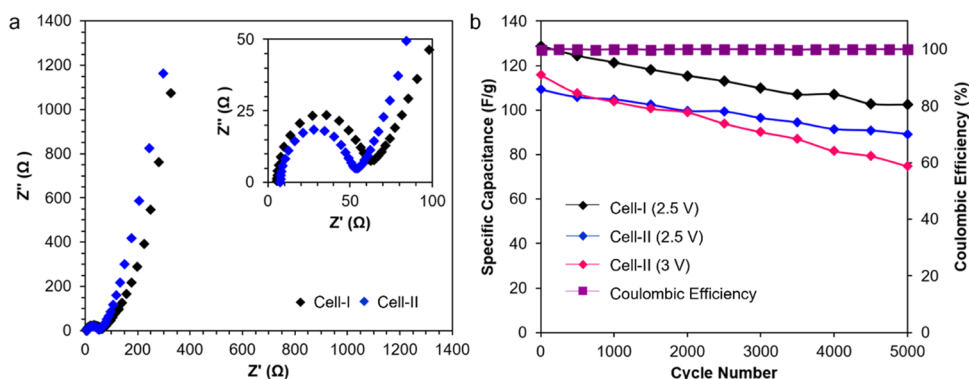


**Figure 5.** (a) Nyquist plot for Cell-I (black) and Cell-II (blue). Inset: Magnified high-frequency region. (b) Cyclic stability of Cell-I and Cell-II at a current density of  $2 \text{ A g}^{-1}$ . Data in black and blue shows the respective cells charging to 2.5 V and data in pink shows Cell-I charging to 3.0 V. Secondary axis shows the Coulombic efficiency (purple) for Cell-II over 5000 cycles.

capacitance for Cell-II was  $130 \text{ F g}^{-1}$  at a current density of  $0.5 \text{ A g}^{-1}$ , about 15% less than that of Cell-I at the same current density. At  $2 \text{ A g}^{-1}$ , the specific capacitance of Cell-II was  $110 \text{ F g}^{-1}$ , whereas that of Cell-I was  $129 \text{ F g}^{-1}$ . The differences in the capacitances of Cell-I and -II are expected due to the lower ionic conductivity in ILGPE because it contains less IL. However, at current densities beyond  $2 \text{ A g}^{-1}$ , the specific capacitances of Cell-I and Cell-II were nearly the same. Interestingly, at  $10 \text{ A g}^{-1}$ , Cell-I stopped working, while Cell-II containing ILGPE-II (the one with calcite) remained operational. It is normal for the specific capacitance to decrease with the increase in current density because of the increasingly restricted movement of the ions into the nanoporous structure of the carbon material.

**Impedance.** Charge-transfer processes and ionic transport of the supercapacitors were investigated by EIS (Figure 5a). There are three parts of the Nyquist plot that are important for determining information about how the device charges and how ions interact at the electrolyte/electrode interface: (i) where the EIS curve intercepts the real axis ( $X$ -axis) is used to estimate the value of the equivalent series resistance (ESR) of the device, (ii) the diameter of the first semicircle provides an estimate of the charge-transfer resistance ( $R_{CT}$ ), and (iii) the behavior of the curve at the lowest frequencies tells us whether our device is a true capacitor. The equivalent series resistance (ESR) is  $6.7$  and  $4.6 \text{ } \Omega$  for Cell-II and -I, respectively. The charge-transfer resistance ( $R_{CT}$ ) was found to be  $46.9 \text{ } \Omega$  for Cell-II and  $57.4 \text{ } \Omega$  for Cell-I. There is a significant difference of more than  $10 \text{ } \Omega$  in the  $R_{CT}$  given the similarity of the ESR between the two films is the evidence that Cell-II has better charge transfer and ion diffusion than Cell-I under these conditions, adding to its stability and rate capability. The differences in charge-transfer resistance between Cell-I and -II led us to investigate differences in the stiffness between ILGPE-I and -II. According to dynamic mechanical analysis (DMA) studies (Supporting Information, Figure S6), at  $25 \text{ } ^\circ\text{C}$ , the storage modulus, loss modulus, and tan delta for the ILGPE-I and -II were  $8.22 \text{ MPa}$ ,  $0.924$ , and  $0.122$  and  $2.80 \text{ MPa}$ ,  $0.654$ , and  $0.233$ , respectively. The storage modulus is a measure of the stiffness of the material; therefore, ILGPE-I is about 3 times stiffer than ILGPE-II. The softness of ILGPE-II and the ease with which it can be compressed (see Video in the Supporting Information) may account for superior electrolyte–electrode contact, which would result in better charge transfer and ion diffusion exhibited by Cell-II by EIS.

Galvanostatic cycling (Figure 5b) of the supercapacitors revealed that Cell-II devices were more stable at 2.5 V as compared to 3 V. Cell-II at 2.5 V and  $2 \text{ A g}^{-1}$  showed good stability, with just an 18.5% drop in specific capacitance and Coulombic efficiency remaining  $>99\%$  after 5000 cycles. Charging to 3 V at a current density of  $2 \text{ A g}^{-1}$  Cell-II was not as stable, with a 35.5% decrease in the specific capacitance despite a high Coulombic efficiency. Cell-I was as stable as Cell-II having a high Coulombic efficiency and a 20.5% decrease in specific capacitance after 5000 cycles. This shows that the incorporation of calcite into the ILGPE films did not decrease the stability or lifetime of the device.

**Ragone Plot.** The Ragone plot (Figure 6) of a supercapacitor is used to show the relationship of energy density

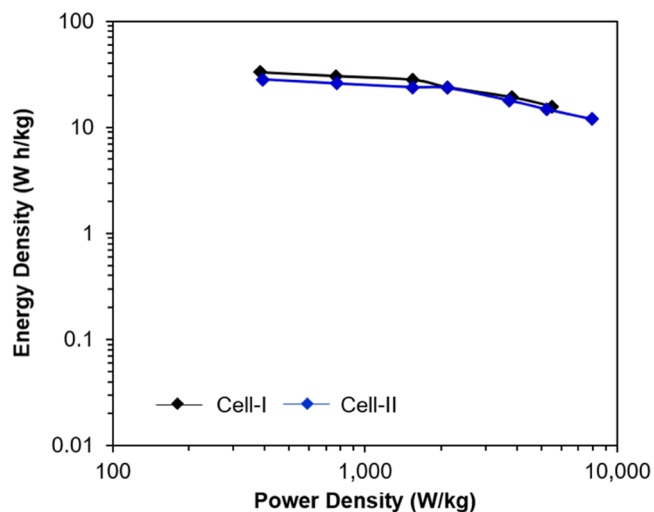


**Figure 6.** Ragone plot for Cell-I (black) and Cell-II (blue) charging to 2.5 V.

power density. Energy ( $E$ ) density and power ( $P$ ) density were calculated using  $E = 1/2 C_{\text{cell}} V^2$  and  $P = E/\Delta t$ , where  $C_{\text{cell}}$  is the specific capacitance of the whole cell,  $V$  is the cell potential, and  $\Delta t$  is the time taken by the supercapacitor to discharge. The highest energy density occurs at the lowest current density and the highest power density occurs at the highest current density. The power and energy density of Cell-I and Cell-II were very similar, meaning that the inorganic calcite filler did not have a detrimental effect on the most critical criteria for the supercapacitor. In fact, because Cell-II could be studied at a

current density of 10 A g<sup>-1</sup> (in terms of the mass of the electrode material), it has a higher power density than Cell-I.

Cell-I had a high energy density of 33.0 Wh/kg at a power density of 0.385 kW/kg. At a higher power density of 5.51 kW/kg, the energy density remained high at 15.6 Wh/kg. Cell-II had a high energy density of 28.2 Wh/kg at a power density of 0.391 kW/kg. Cell-II had the highest power density of 8.81 kW/kg at an energy density of 8.1 Wh/kg. Cell-II is superior to a closely related supercapacitor system that contains an ILGPE made up of EMIM TFSI/PVdF-HFP/Zeolite (70:28:2) that had its highest power density of 2.73 kW/kg at the same 10 A g<sup>-1</sup>.<sup>10</sup> This is likely due to differences in the amount of polymer in the ILGPE and the surface area of active carbon.

The real comparison we want to make in this manuscript is between the two supercapacitors fabricated with and without calcite because it is difficult to compare with other systems when there are many differences including the mass of active material, electrolyte (IL), thickness of the electrolyte, etc. The power and energy densities of Cell-I and -II were not dramatically different and are both within standards of what is typical of an electrochemical supercapacitor.<sup>2</sup>

## CONCLUSIONS

In summary, the addition of a biorenewable calcite into the ILGPE resulted in films that are free-standing, flexible, and mechanically strong. Both ILGPEs were thermally stable up to 350 °C and had a maximum cell potential of 3.5 V. When part of a symmetric coin cell capacitor, ILGPE-II showed no consequence of stability or lifetime of the device. In some instances, calcite proved beneficial. Cell-II had a smaller R<sub>CT</sub> and better retention of specific capacitance (81.5%) after 5000 cycles in comparison to Cell-I. Neither the electrochemical window nor capacitance behavior was altered by the addition of a biorenewable calcite. The specific capacitance and energy density of Cell-II were very similar to those of Cell-I, and still well within the standards for activated carbon supercapacitors. Cell-II had higher power density (able to withstand higher current density) than Cell-I. The maximum energy density and power density of Cell-II were 28 Wh/kg and 8.1 kW/kg at 0.5 and 10 A g<sup>-1</sup>, respectively. This research is promising for the development of solid-state electrolytes for supercapacitors like ILGPEs because the biorenewable calcite enhanced the mechanical stability of ILGPEs and decreased the cost. The small amount of volume of the calcite added allowed one to two more ILGPEs per standard batch of ILGPE-II in comparison to ILGPE-I. This biorenewable inorganic additive, which would have ended up in a landfill, decreased the cost of the supercapacitor by up to 17%. ILGPE-II, which contained calcite, was more mechanically stable and better suited for a supercapacitor in our opinion because it was compressible (a characteristic of the calcite material itself) and was not as stiff as ILGPE-I.

## ASSOCIATED CONTENT

### Supporting Information

The Supporting Information is available free of charge at <https://pubs.acs.org/doi/10.1021/acsomega.2c06876>.

Arrhenius plot, DSC curves, SEM images, and dynamic mechanical analysis of ILGPE-I and ILGPE-II, and cyclic voltammograms of Cell-I (PDF)

Softness of ILGPE-II and ease with which it can be compressed may account for superior electrolyte–

electrode contact, which would result in better charge transfer and ion diffusion exhibited by Cell-II by EIS (MOV)

## AUTHOR INFORMATION

### Corresponding Author

Jennifer N. Murphy – ARC Centre of Excellence for Electromaterials Science, School of Chemistry, Monash University, Clayton, Victoria 3800, Australia; Department of Chemistry, Memorial University, St. John's, Newfoundland A1B 3X7, Canada; Present Address: Department of Chemistry, University of Guelph, Guelph, Ontario N1G 2W1, Canada; [orcid.org/0000-0001-6938-1137](https://orcid.org/0000-0001-6938-1137); Email: [jennifer.n.murphy@mun.ca](mailto:jennifer.n.murphy@mun.ca)

### Authors

Tiago Mendes – ARC Centre of Excellence for Electromaterials Science, School of Chemistry, Monash University, Clayton, Victoria 3800, Australia; ARC Centre of Excellence for Electromaterials Science, Institute for Frontier Materials, Deakin University, Burwood, Victoria 3125, Australia; [orcid.org/0000-0003-2436-4864](https://orcid.org/0000-0003-2436-4864)

Francesca M. Kerton – Department of Chemistry, Memorial University, St. John's, Newfoundland A1B 3X7, Canada; [orcid.org/0000-0002-8165-473X](https://orcid.org/0000-0002-8165-473X)

Douglas R. MacFarlane – ARC Centre of Excellence for Electromaterials Science, School of Chemistry, Monash University, Clayton, Victoria 3800, Australia; [orcid.org/0000-0001-5963-9659](https://orcid.org/0000-0001-5963-9659)

Complete contact information is available at:

<https://pubs.acs.org/10.1021/acsomega.2c06876>

### Notes

The authors declare no competing financial interest.

## ACKNOWLEDGMENTS

The authors thank NSERC of Canada, CFI, RDC-NL, and Memorial University (MUN) for funding.

## REFERENCES

- (1) Armand, M.; Tarascon, J. M. Building better batteries. *Nature* **2008**, *451*, 652–657. Article
- (2) Simon, P.; Gogotsi, Y. Materials for electrochemical capacitors. *Nat. Mater.* **2008**, *7*, 845–854. Review
- (3) (a) Conway, B. E. *Electrochemical Supercapacitors: Scientific Fundamentals and Technological Applications*; Springer US, 1999. (b) Miller, J. R.; Simon, P. Materials science - Electrochemical capacitors for energy management. *Science* **2008**, *321*, 651–652. Editorial Material
- (4) Kaempgen, M.; Chan, C. K.; Ma, J.; Cui, Y.; Gruner, G. Printable thin film supercapacitors using single-walled carbon nanotubes. *Nano Lett.* **2009**, *9*, 1872–1876.
- (5) Armand, M.; Endres, F.; MacFarlane, D. R.; Ohno, H.; Scrosati, B. Ionic-liquid materials for the electrochemical challenges of the future. *Nat. Mater.* **2009**, *8*, 621–629.
- (6) Pandey, G. P.; Hashmi, S. A. Ionic liquid 1-ethyl-3-methylimidazolium tetracyanoborate-based gel polymer electrolyte for electrochemical capacitors. *J. Mater. Chem. A* **2013**, *1*, 3372–3378.
- (7) Guo, N.; Li, M.; Wang, Y.; Sun, X.; Wang, F.; Yang, R. Soybean Root-Derived Hierarchical Porous Carbon as Electrode Material for High-Performance Supercapacitors in Ionic Liquids. *ACS Appl. Mater. Interfaces* **2016**, *8*, 33626–33634.
- (8) Sillars, F. B.; Fletcher, S. I.; Mirzaeian, M.; Hall, P. J. Variation of electrochemical capacitor performance with room temperature ionic

liquid electrolyte viscosity and ion size. *Phys. Chem. Chem. Phys.* **2012**, *14*, 6094–6100.

(9) (a) Kang, Y. J.; Chun, S.-J.; Lee, S.-S.; Kim, B.-Y.; Kim, J. H.; Chung, H.; Lee, S.-Y.; Kim, W. All-Solid-State Flexible Supercapacitors Fabricated with Bacterial Nanocellulose Papers, Carbon Nanotubes, and Triblock-Copolymer Ion Gels. *ACS Nano* **2012**, *6*, 6400–6406. (b) Jiang, J.; Gao, D.; Li, Z.; Su, G. Gel polymer electrolytes prepared by in situ polymerization of vinyl monomers in room-temperature ionic liquids. *React. Funct. Polym.* **2006**, *66*, 1141–1148. (c) Lewandowski, A.; Swiderska, A. New composite solid electrolytes based on a polymer and ionic liquids. *Solid State Ionics* **2004**, *169*, 21–24. (d) Sutto, T. E. The electrochemical behavior of trialkylimidazolium imide based ionic liquids and their polymer gel electrolytes. *J. Electrochem. Soc.* **2007**, *154*, P130–P135.

(10) Lu, W.; Henry, K.; Turchi, C.; Pellegrino, J. Incorporating ionic liquid electrolytes into polymer gels for solid-state ultracapacitors. *J. Electrochem. Soc.* **2008**, *155*, A361–A367.

(11) (a) Nohara, S.; Wada, H.; Furukawa, N.; Inoue, H.; Morita, M.; Iwakura, C. Electrochemical characterization of new electric double layer capacitor with polymer hydrogel electrolyte. *Electrochim. Acta* **2003**, *48*, 749–753. Article (b) Yang, C. M.; Ju, J. B.; Lee, J. K.; Cho, W. L.; Cho, B. W. Electrochemical performances of electric double layer capacitor with UV-cured gel polymer electrolyte based on poly(ethylene glycol)diacrylate-poly(vinylidene fluoride) blend. *Electrochim. Acta* **2005**, *50*, 1813–1819. Article

(12) Nunes-Pereira, J.; Costa, C. M.; Lanceros-Mendez, S. Polymer composites and blends for battery separators: State of the art, challenges and future trends. *J. Power Sources* **2015**, *281*, 378–398.

(13) (a) Mirzaeian, M.; Abbas, Q.; Ogwu, A.; Hall, P.; Goldin, M.; Mirzaeian, M.; Jirandehi, H. F. Electrode and electrolyte materials for electrochemical capacitors. *Int. J. Hydrogen Energy* **2017**, *42*, 25565–25587. (b) Pal, P.; Ghosh, A. Solid-state gel polymer electrolytes based on ionic liquids containing imidazolium cations and tetrafluoroborate anions for electrochemical double layer capacitors: Influence of cations size and viscosity of ionic liquids. *J. Power Sources* **2018**, *406*, 128–140.

(14) Zhang, X.; Kar, M.; Mendes, T. C.; Wu, Y.; MacFarlane, D. R. Supported Ionic Liquid Gel Membrane Electrolytes for Flexible Supercapacitors. *Adv. Energy Mater.* **2018**, *8*, No. 1702702.

(15) (a) Ortega, P. F. R.; Trigueiro, J. P. C.; Silva, G. G.; Lavall, R. L. Improving supercapacitor capacitance by using a novel gel nano-composite polymer electrolyte based on nanostructured SiO<sub>2</sub>, PVDF and imidazolium ionic liquid. *Electrochim. Acta* **2016**, *188*, 809–817. (b) Ketabi, S.; Lian, K. Effect of SiO<sub>2</sub> on conductivity and structural properties of PEO-EMIHSO<sub>4</sub> polymer electrolyte and enabled solid electrochemical capacitors. *Electrochim. Acta* **2013**, *103*, 174–178.

(16) Lavall, R. L.; Ferrari, S.; Tomasi, C.; Marzantowicz, M.; Quartarone, E.; Fagnoni, M.; Mustarelli, P.; Saladino, M. L. MCM-41 silica effect on gel polymer electrolytes based on thermoplastic polyurethane. *Electrochim. Acta* **2012**, *60*, 359–365.

(17) (a) Gong, Y.; Li, D.; Luo, C.; Fu, Q.; Pan, C. Highly porous graphitic biomass carbon as advanced electrode materials for supercapacitors. *Green Chem.* **2017**, *19*, 4132–4140. (b) Yadav, N.; Singh, M. K.; Yadav, N.; Hashmi, S. A. High performance quasi-solid-state supercapacitors with peanut-shell-derived porous carbon. *J. Power Sources* **2018**, *402*, 133–146.

(18) Murphy, J. N.; Schneider, C. M.; Hawboldt, K.; Kerton, F. M. Hard to Soft: Biogenic Absorbent Sponge-Like Material from Waste Mussel Shells. *Matter* **2020**, *3*, 2029–2041.

(19) Tamilarasan, P.; Ramaprabhu, S. Graphene based all-solid-state supercapacitors with ionic liquid incorporated polyacrylonitrile electrolyte. *Energy* **2013**, *51*, 374–381.

(20) (a) Lewandowski, A.; Swiderska, A. Electrochemical capacitors with polymer electrolytes based on ionic liquids. *Solid State Ionics* **2003**, *161*, 243–249. (b) Tafur, J. P.; Fernandez Romero, A. J. Electrical and spectroscopic characterization of PVdF-HFP and TFSI ionic liquid-based gel polymer electrolyte membranes. Influence of ZnTf<sub>2</sub> salt. *J. Membr. Sci.* **2014**, *469*, 499–506. (c) Guisao, J. P. T.; Romero, A. J. F. Interaction between Zn<sup>2+</sup> cations and n-methyl-2-

pyrrolidone in ionic liquid-based Gel Polymer Electrolytes for Zn batteries. *Electrochim. Acta* **2015**, *176*, 1447–1453. (d) Pandey, G. P.; Kumar, Y.; Hashmi, S. A. Ionic liquid incorporated PEO based polymer electrolyte for electrical double layer capacitors: A comparative study with lithium and magnesium systems. *Solid State Ionics* **2011**, *190*, 93–98.

(21) (a) Zhang, S. S.; Xu, K.; Jow, T. R. An inorganic composite membrane as the separator of Li-ion batteries. *J. Power Sources* **2005**, *140*, 361–364. (b) Liu, H. Y.; Liu, L. L.; Yang, C. L.; Li, Z. H.; Xiao, Q. Z.; Lei, G. T.; Ding, Y. H. A hard-template process to prepare three-dimensionally macroporous polymer electrolyte for lithium-ion batteries. *Electrochim. Acta* **2014**, *121*, 328–336.

(22) Xyla, A. G.; Koutsoukos, P. G. Quantitative Analysis of Calcium Carbonate Polymorphs by Infrared Spectroscopy. *J. Chem. Soc., Faraday Trans. 1* **1989**, *85*, 3165–3172.